Electronic supplementary information

Design of molecular sensors and switches based on luminescent ruthenium-terpyridine complexes bearing active methylene and triphenylphosphonium motifs as the anion recognition sites: experimental and DFT/ TD-DFT investigation

Sohini Bhattacharya[a], Poulami Pal[a,b], and Sujoy Baitalik [a*]

[a] Department of Chemistry, Inorganic Chemistry Section, Jadavpur University, Kolkata 700032, India.

[b] School of Chemical Sciences, Indian Association for the Cultivation of Science, 2A & B Raja S C Mullick Road, Kolkata 700032, India

Experimental section

$RuCl_3 \cdot xH_2O$ was purchased from Sigma Aldrich. Other analytical reagent grade chemicals as well as solvents were procured from local vendors. The precursors that were used for the synthesis of the ligands such as 4′-(p-methylphenyl)-2,2′:6′,2″-terpyridine (tpy-$PhCH_3$), 4′-(p-bromomethyl phenyl)-2,2′:6′,2″-terpyridine (tpy-$PhCH_2Br$) and 4′(2,2′:6′,2″-terpyridyl-4)-benzyltriphenyl phosphonium bromide (tpy-$PhCH_2PPh_3Br$) were synthesized following reported literature procedures.[S1] [(tpy-$PhCH_3$)$RuCl_3$] was prepared by refluxing $RuCl_3 \cdot 3H_2O$ and tpy-$PhCH_3$ (1:1 molar ratio) in EtOH.

Synthesis of the ligand (tpy-$PhCH_2PPh_3Br$)

Prepared following the procedure mentioned in literature.[S1]

Synthesis of the metal complexes

The complexes were prepared under oxygen and moisture free inert atmosphere using standard Schlenk techniques.

A procedure as described below was adopted for the synthesis of the complexes.

[(tpy-$PhCH_3$)Ru(tpy-$PhCH_2PPh_3Br$)]$(ClO_4)_2$ (1H)

In this case [Ru(tpy-$PhCH_3$)Cl_3] (0.53g,0.18mmole) and tpy-$PhCH_2PPh_3Br$ (0.66 g, 0.18 mmole) were mixed in 5-8 mL ethylene glycol stirred under refluxing condition in an inert condition for overnight. The red compound that deposited upon cooling was collected by filtration. Acetonitrile solution of the resulting compound was subjected to column chromatography (silica gel) and eluted with MeCN−$PhCH_3$ (10:1, v/v) mixture. The desired compound was collected upon evaporation to a small volume. Recrystallization of the complex from MeCN−MeOH (1:1, v/v) mixture was done for further purification. Crystalline red coloured compound was collected (126 mg, yield, 52%). Anal. Calcd for $C_{62}H_{48}N_6PBrCl_2O_8Ru$: C, 57.76; H, 3.72; N, 8.00 Found: C, 57.71; H, 3.74; N, 8.05%. ^{1}H NMR {400 MHz, deuterated dimethyl sulfoxide (DMSO-d_6)}: δ 9.46 (s, 2H, H3′), 9.43 (s, 2H, H3′″), 9.11 (d, 2H, J = 8 Hz, H6), 9.05 (d, 2H, J = 8 Hz, H6′), 8.37 (d, 4H, J = 8 Hz, H7 & H7′), 8.06 (d, 2H, J = 7.84 Hz, H4, H4′), 7.99 (t, 2H, J = 7.16 Hz, H12 & H17), 7.76−7.86 (m, 15H, H10, H11, H13-H16), 7.5-7.6 (m, 6H, H8,H3,H3″), 7.34 (d, 2H, J = 8 Hz, H8′), 7.24−7.3 (m, 4H, H5 & H5′), 5.36 (d, 2H, J = 16 Hz, H9), 2.52 (s, 3H, H10). Electrospray ionization mass spectrometry (ESI-MS; positive, MeCN) m/z = 336.43 (100%) [(tpy-

$PhCH_3$)Ru(tpy-$PhCH_2PPh_3Br$)]$^{3+}$and m/z=373.61 (40%) [(tpy-$PhCH_3$)Ru(tpy-$PhCH_2PPh_3Br$)]$^{2+}$.

[Ru(tpy-$PhCH_2PPh_3Br)_2$]$(ClO_4)_2$ (2H)

$Ru(DMSO)_4Cl_2$ (0.55g, 0.11mmol) and tpy-$PhCH_2PPh_3Br$ (1.5g, 0.22mmol) were taken in 1:2 molar ratio in ethylene glycol and refluxed for 3h. The compound was purified successively by silica gel column chromatography as well as recrystallization from MeCN-MeOH (1:1, v/v). Yield = 92 mg (49%): Anal. Calcd. for $C_{80}H_{62}N_6P_2Br_2Cl_2O_8Ru$: C, 63.30; H, 3.98; N, 10.25. Found: C, 63.24; H, 3.95; N, 10.30%. 1H NMR (500 MHz, deuterated dimethyl sulfoxide (DMSO-d_6)): δ 9.43 (s, 4H, H3′), 9.048 (d, 4H, J = 8Hz, H6), 8.36 (d, 4H, J = 7.5 Hz, H7), 8.06 (t, 4H, J = 7.75 Hz, H4), 7.97 (t, 6H, J = 7 Hz, H12 & H17), 7.76-7.85 (m, 24H, H-10,11,13-16), 7.51 (d, 4H, J = 5.5 Hz, H8), 7.34 (d, 4H, J = 7 Hz, H3), 7.26 (t, 4H, J = 6.5 Hz, H5), 5.35(d, 2H, J = 15 Hz, H9) Electrospray ionization mass spectrometry (ESI-MS; positive, MeCN) m/z = 317.59 (34%) [Ru(tpy- PhCH2PPh3Br)2]$^{4+}$, m/z = 336.09 (100%) [Ru(tpy- $PhCH_2PPh_3Br)_2$]$^{3+}$ and m/z = 373.16 (28%) [Ru(tpy- $PhCH_2PPh_3Br)_2$]$^{2+}$

Caution! Perchlorate salts of the metal complexes are explosive and should be handled in small amount with extreme care

Physical measurements.

Elemental analyses of the compounds were performed with a Vario-Micro V2.0.11 elemental (CHNSO) analyzer. NMR spectra were collected on a Bruker 400 MHz spectrometer in DMSO-d_6. High resolution mass spectrometry was performed on a Waters Xevo G2 QTOf mass spectrometer. UV-vis absorption spectra of the complexes were recorded with a Shimadzu UV 1800 spectrometer. Steady state luminescence spectra were obtained by a Horiba Fluoromax-4 spectrometer. Luminescence quantum yields were determined by using literature method taking [Ru(bpy)$_3$]$^{2+}$as the standard. Luminescence lifetime measurements were carried out by using time–correlated single photon counting set up from Horiba Jobin-Yvon. The luminescence decay data were collected on a Hamamatsu MCP photomultiplier (R3809) and were analyzed by using IBH DAS6 software. Spectrophotometric titrations were carried out with a series of DMSO solutions containing the same amount of complex (1.5×10^{-5} M).

Electrochemical measurements were carried out in deaerated acetonitrile with a BAS epsilon electrochemistry system and a three-electrode set up consisting of a platinum or

glassy carbon working electrode, a platinum counter electrode, and Ag/AgCl reference electrode. In all the experiments, tetraethylammonium perchlorate (TEAP) was used as background electrolyte. The potentials reported in this study were referenced against the Ag/AgCl electrode, which under the given experimental conditions gave a value of 0.36 V for the Fc/Fc+ couple.

Experimental uncertainties are as follows: absorption maxima, ±2 nm; molar absorption coefficients, 10%; emission maxima, ±5 nm; excited–state lifetimes, 10%; luminescence quantum yields, 20%.

Computational methods

All calculations were performed with the Gaussian 09 program[S2] employing the DFT method with Becke's three-parameter hybrid functional and LeeYang-Parr's gradient corrected correlation functional B3LYP level of theory.[S3-S4] 6-31G(d) basis set was employed for the C, H, N, Br and O while SDD basis set was used for Ru atom.[S5] Geometries were fully optimized using the criteria of the respective programs. TD-DFT[S6-S9] calculations of the singlet-singlet excitations were performed in DMSO simulated by the CPCM model[S10] by using the so-called non-equilibrium approach, which has been designed for the study of the absorption process.[S11-S12] Orbital analysis was completed with Gauss View[S13] and Gauss sum 2.2.[S14]

Tables for electronic supplementary information

Table S1. Selected MOs along with their energies and compositions in the ground state of the complex, **1H** and it's deprotonated form, $\mathbf{1^-}$ in DMSO.

MO	Energy/eV		% Compositions				% Compositions			
	1H	$\mathbf{1^-}$	**1H**				$\mathbf{1^-}$			
			Ru	mpt	methphos	phetpy	Ru	mpt	methphos	phetpy
LUMO+5	-1.6	-1.48	0.54	0.23	53.26	45.95	1.55	98.50	0.00	0.00
LUMO+4	-1.78	-1.5	0.18	0.02	64.25	35.53	0.00	53.38	0.00	46.59
LUMO+3	-2.42	-2.25	2.92	70.79	0.00	26.26	2.55	8.28	0.00	89.14
LUMO+2	-2.51	-2.39	0.17	27.64	0.01	72.16	0.70	90.01	0.00	9.26
LUMO+1	-2.65	-2.45	7.77	90.25	0.00	1.96	6.75	1.34	3.14	88.75
LUMO	-2.72	-2.57	8.13	2.04	0.97	88.84	8.42	90.04	0.00	1.52
HOMO	-6.09	-4.63	60.12	33.1	0.00	6.69	3.72	0.00	50.01	45.80
HOMO-1	-6.14	-5.94	68.35	12.29	0.21	19.13	62.52	30.53	0.00	6.93
HOMO-2	-6.15	-5.99	67.46	10.12	0.35	22.05	70.00	14.78	0.00	15.19
HOMO-3	-6.91	-6.04	12.69	85.72	0.00	1.58	65.46	7.15	5.06	72.32
HOMO-4	-7.17	-6.85	0.00	99.50	0.08	0.41	9.98	88.71	0.00	1.28
HOMO-5	-7.22	-6.89	6.10	1.42	17.02	75.44	0.00	0.00	3.72	95.99

Table S2. Selected MOs along with their energies and compositions in the ground state of the complex, **2H** and it's deprotonated form, $\mathbf{2^-}$ in DMSO.

MO	Energy/eV		% Compositions			% Compositions		
	2H	$\mathbf{2^-}$	**2H**			$\mathbf{2^-}$		
			Ru	methphos	phetpy	Ru	methphos	phetpy
LUMO+5	-1.79	-1.39	0.20	59.25	40.53	1.71	5.72	92.55
LUMO+4	-1.79	-1.45	0.22	58.97	40.80	0.00	0.00	99.99
LUMO+3	-2.48	-2.18	3.06	0.00	96.91	3.37	0.00	96.61
LUMO+2	-2.56	-2.26	0.00	0.00	99.97	0.00	0.00	99.98
LUMO+1	-2.75	-2.4	7.98	0.97	91.03	7.21	3.08	89.70
LUMO	-2.76	-2.4	8.01	0.97	91.01	7.22	3.08	89.69
HOMO	-6.19	-4.59	65.59	0.59	33.80	4.18	49.30	46.50
HOMO-1	-6.19	-4.61	69.08	0.11	30.80	4.25	49.85	45.89
HOMO-2	-6.2	-5.89	66.36	0.49	33.13	70.09	0.05	29.84
HOMO-3	-7.24	-5.93	6.43	17.12	76.44	65.51	5.07	29.40
HOMO-4	-7.24	-5.93	6.70	17.30	75.98	65.33	5.18	29.48
HOMO-5	-7.28	-6.87	0.03	0.08	99.88	0.00	4.24	95.69

Table S3. Selected UV-vis energy transitions at the TD-DFT/B3LYP level of complex, **1** and it's deprotonated form, **1**$^-$ in DMSO.

Excited State	λ_{cal}/nm	Oscillator Strength(f)	λ_{expt}/nm	Key transitions	Character
1H					
S_2	493	0.0123	497	H-2→L (35%), H-1→L (62%)	MLCT
S_3	481	0.0134		H-2→L+1 (27%), H-1→L+1 (71%)	
S_5	461	0.4301	451	H-2→L (33%), H-1→L (18%), H→L+1 (41%), H-1→L+2 (3%)	MLCT, ILCT
S_{10}	421	0.2119		H-2→L+2 (23%), H-1→L+2 (55%), H-1→L+3 (15%), H-2→L (3%)	
S_{14}	331	0.264	335	H-3→L+1 (84%), H-3→L (3%), H-2→L+6 (3%), H-1→L+6 (6%)	π-π*, MLCT
S_{25}	322	0.103		H-2→L+6 (11%), H-1→L+6 (15%), H→L+7 (64%), H-3→L+1 (4%)	
S_{28}	313	0.219	316	H-6→L (61%), H-5→L+2 (3%), H-4→L (5%), H-2→L+4 (6%), H-1→L+4 (9%)	ILCT, π-π*
S_{30}	310	0.2749		H-5→L (87%), H-1→L+6 (2%)	
S_{38}	30	0.2603	291	H-7→L+1 (78%), H-3→L+3 (4%), H-2→L+7 (5%), H-1→L+7 (7%)	π-π*, ILCT
S_{62}	279	0.8295		H-7→L+2 (19%), H-6→L+3 (52%), H-8→L+2 (3%), H-5→L+3 (4%), H-2→L+9 (4%), H-1→L+9 (3%)	
1$^-$					
S_2	659	0.7043	605	H→L+1 (97%)	ILCT
S_5	495	0.0141	498	H-2→L (97%)	MLCT
S_9	461	0.2522		H-2→L+2 (13%), H-1→L (70%), H-3→L+1 (5%), H-2→L+3 (3%), H→L+6 (4%)	
S_{18}	422	0.1056	409	H-2→L+2 (42%), H-2→L+3 (10%), H-1→L+3 (33%), H-1→L (6%), H→L+6 (3%)	MLCT
S_{22}	391	0.4619		H→L+11 (87%), H→L+8 (3%), H→L+12 (5%)	
S_{33}	330	0.2597	334	H-4→L (38%), H-2→L+4 (38%), H-1→L+5 (22%)	π-π*
S_{50}	306	0.0859	318	H-6→L (20%), H-5→L (50%), H-9→L (3%), H-7→L (6%), H-2→L+5 (4%), H→L+16 (9%)	ILCT
S_{53}	304	0.4282		H-6→L+1 (66%), H-2→L+6 (16%), H-9→L (2%), H-5→L+3 (3%)	

Table S4. Selected UV-vis energy transitions at the TD-DFT/B3LYP level of complex, **2H** and it's deprotonated form, **2**$^-$ in DMSO.

Excited State	λ_{cal}/nm	Oscillator Strength (f)	λ_{expt}/nm	Key transitions	Character
2H					
S_4	490	0.0121	497	H-2→L+1 (41%), H→L (49%), H-1→L+1 (7%)	MLCT
S_5	460	0.4725	447	H-2→L (39%), H→L+1 (46%), H-1→L (9%), H-1→L+2 (4%)	MLCT
S_7	427	0.0266		H→L+2 (94%), H-2→L+3 (3%)	
S_{20}	324	0.5536	337	H-2→L+4 (27%), H-2→L+7 (15%), H→L+5 (12%), H-2→L+6 (4%)	MLCT, ILCT
S_{24}	322	0.0569		H-2→L+6 (15%), H-1→L+6 (58%), H-4→L (2%),	
S_{26}	312	0.3184	317	H-5→L+1 (52%), H-1→L+4 (17%), H-4→L+2 (4%), H→L+13 (6%)	π-π*
S_{28}	310	0.4922		H-4→L (45%), H-3→L+1 (44%), H-1→L+6 (6%)	π-π*
S_{33}	302	0.1239	306	H-2→L+4 (12%), H→L+5 (21%), H→L+8 (13%), H→L+14 (12%), H-2→L+7 (8%)	π-π*
S_{41}	296	0.0751		H-4→L+3 (23%), H-3→L+2 (50%), H-8→L+1 (5%), H-7→L (4%)	
S_{47}	289	0.0644	293	H-2→L+7 (12%), H→L+8 (20%), H→L+9 (11%), H→L+14 (14%)	π-π*, ILCT
2$^-$					
S_1	675	1.0452	630	H-1→L (31%), H→L (51%), H→L+1 (14%)	ILCT
S_{14}	450	0.2205	403	H-1→L+5 (29%), H-1→L+7 (58%)H-1→L+10 (5%), H→L+8 (2%)	MLCT, ILCT
S_{17}	443	0.2208		H-4→L (23%), H-3→L+1 (17%), H→L+6 (33%), H-3→L (3%), H-2→L+2 (4%), H-1→L+7 (5%)	
S_{33}	391	0.4608		H-1→L+12 (87%), H-1→L+7 (3%)	
S_{42}	364	0.2622	361	H-1→L+15 (13%), H-1→L+17 (12%), H→L+14 (12%), H→L+16 (56%)	π-π*
S_{44}	358	0.084		H-1→L+15 (55%), H-1→L+17 (36%),H-1→L+12 (3%), H-1→L+21 (3%)	
S_{52}	335	0.0365	330	H-1→L+21 (89%),H-1→L+15 (2%), H-1→L+22 (3%)	π-π*
S_{74}	305	0.1589	315	H-7→L (55%), H→L+23 (10%), H-6→L (3%), H-6→L+1 (6%), H-5→L (2%), H-4→L+9 (3%)	π-π*
S_{76}	304	0.071		H-7→L (15%), H-7→L+1 (4%), H-3→L+19 (9%), H-3→L+26 (3%), H→L+25 (4%)	

Figures for electronic supplementary information

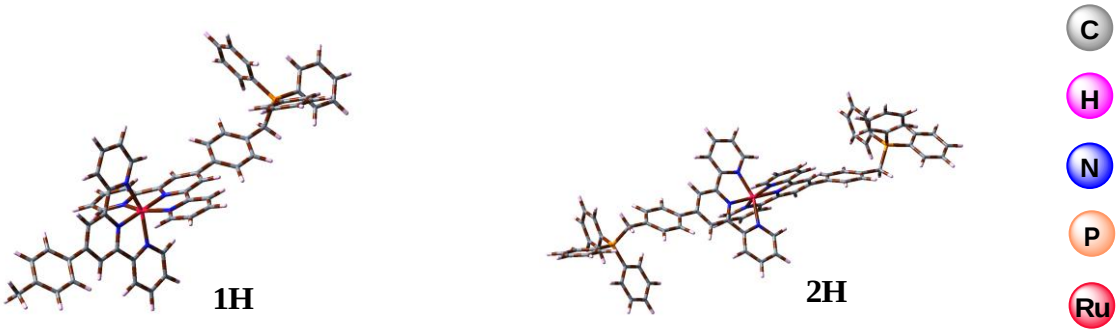

Fig. S1 Optimised structure of **1H** and **2H** in DMSO.

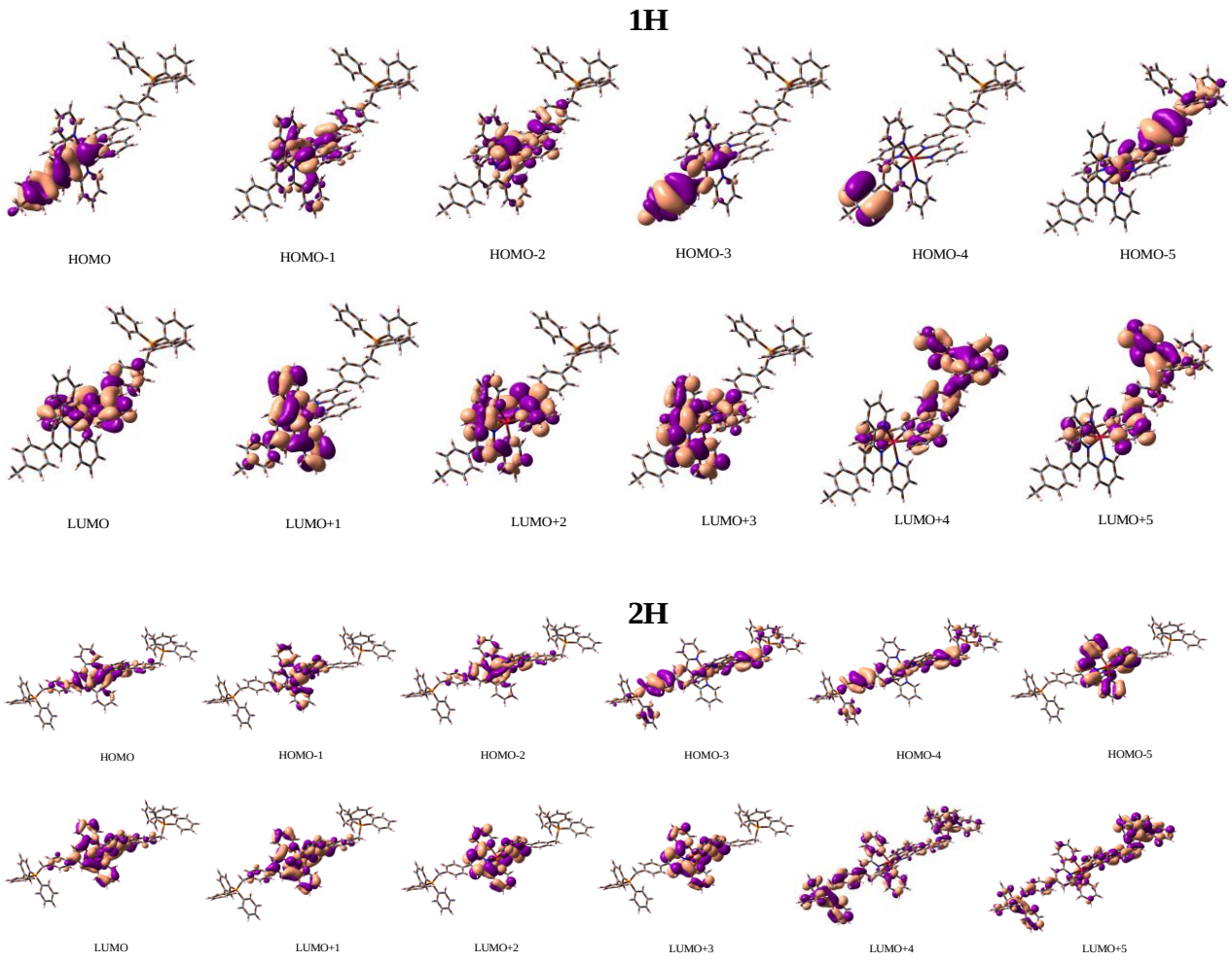

Fig. S2 Schematic drawings of the selective frontier molecular orbitals of complex **1H** and **2H** in DMSO.

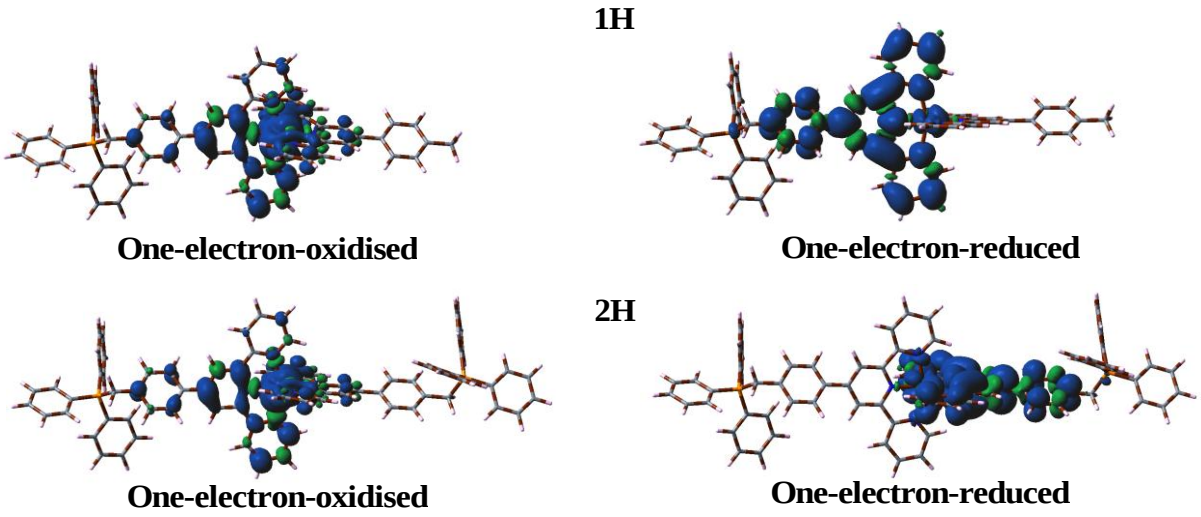

Fig. S3 Spin density plot for **1H** and **2H** in acetonitrile where left side denotes one-electron-oxidised and right side denotes one-electron-reduced form.

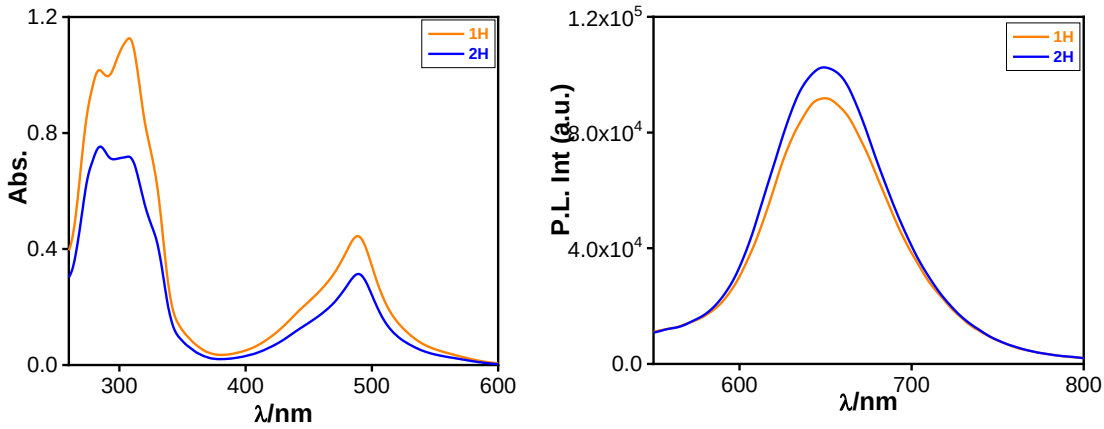

Fig. S4 (a) Absorption and (b) luminescence spectra of **1H** and **2H** in MeCN. The emission was recorded upon excitation at 490 nm.

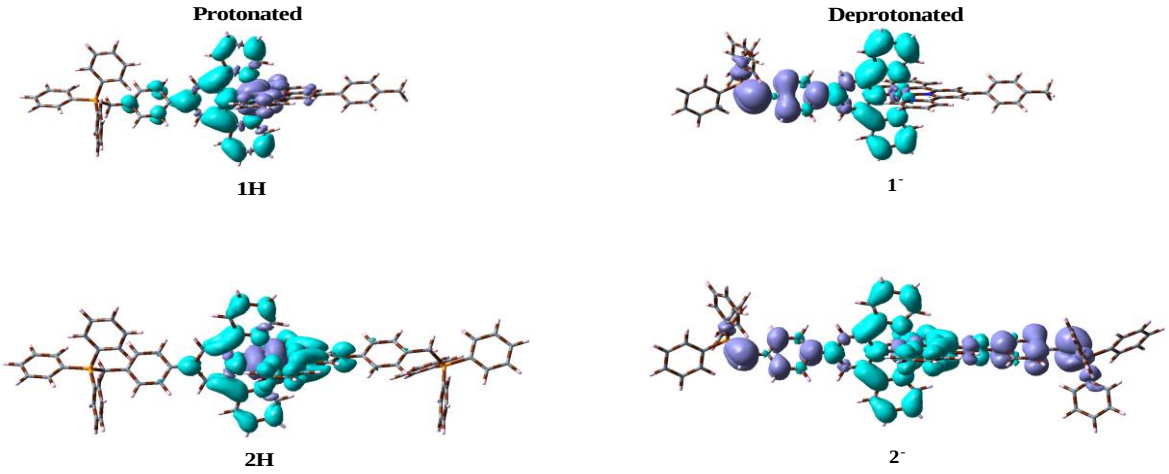

Fig. S5 Difference in electron density upon excitation from the ground S_0 state to the lowest energy singlet excited state in protonated (**1H** and **2H**) and deprotonated ($\mathbf{1}^-$ and $\mathbf{2}^-$) forms of complexes. Purple and cyan color shows regions of increasing and decreasing electron density, respectively.

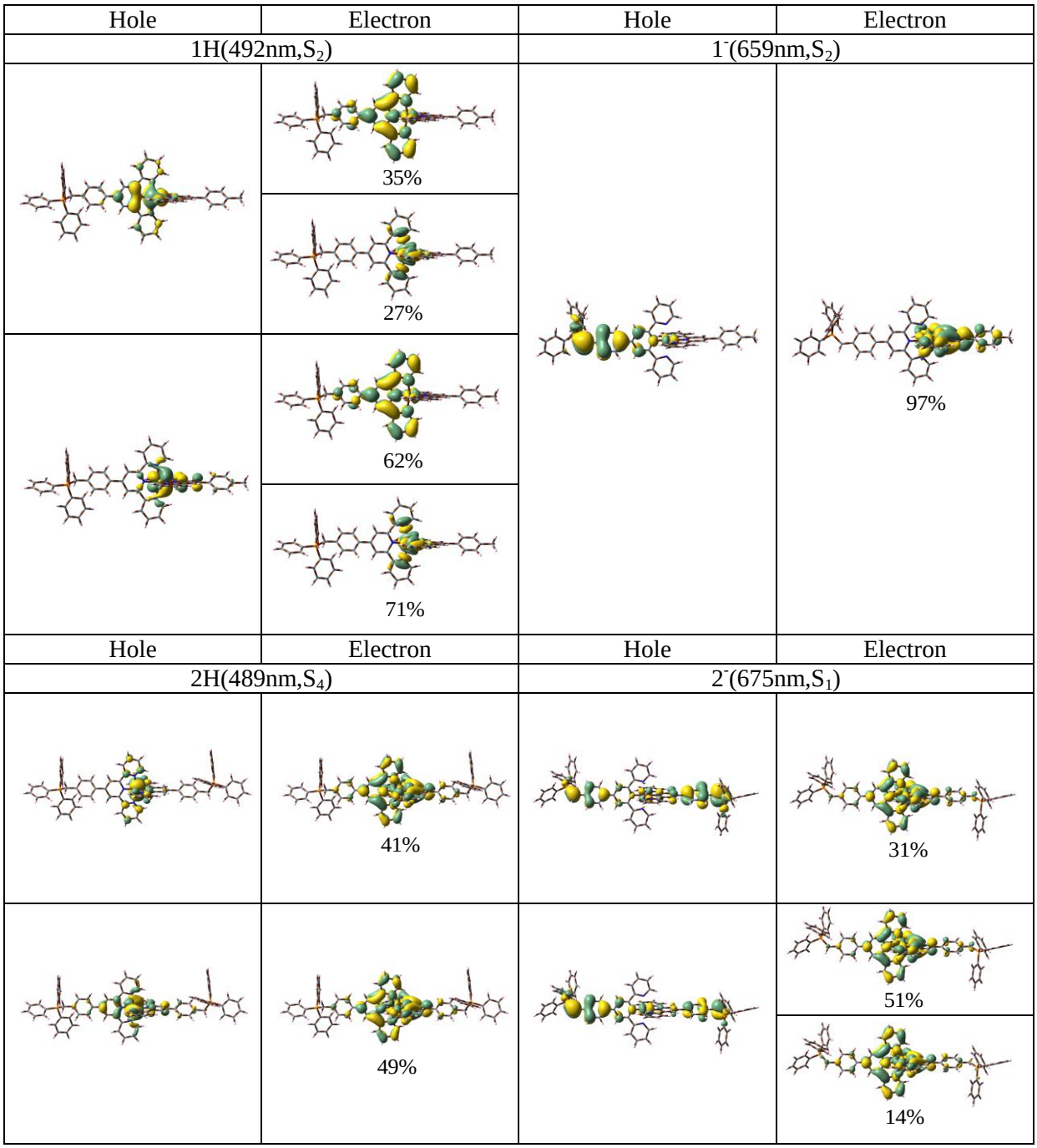

Fig. S6 NTOs illustrating the nature of optically active lowest energy singlet excited states in the absorption bands of the complex **1H** and **2H** in their protonated and deprotonated (**1**$^{-}$ and **2**$^{-}$) forms. The occupied (holes) and unoccupied (electrons) NTO pairs that contribute more than 10% to each excited state are only represented.

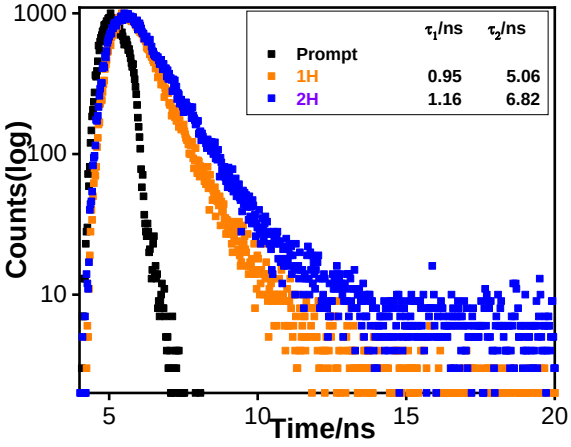

Fig. S7 Excited state decay profiles of **1H** and **2H** in MeCN upon excitation with 450 nm NanoLED. The inset shows the lifetime.

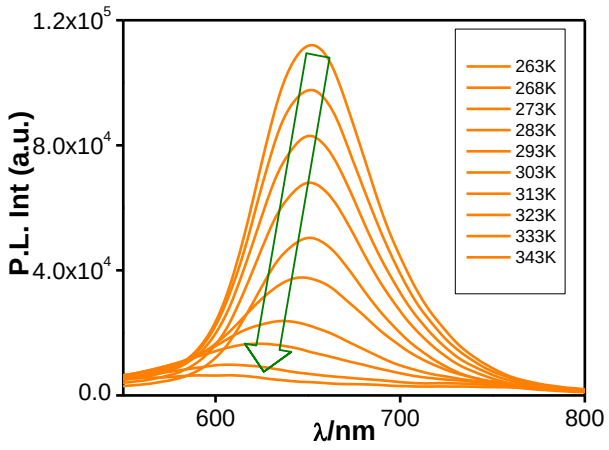

Fig. S8 Emission spectral change of **1H** in MeCN upon varying temperature.

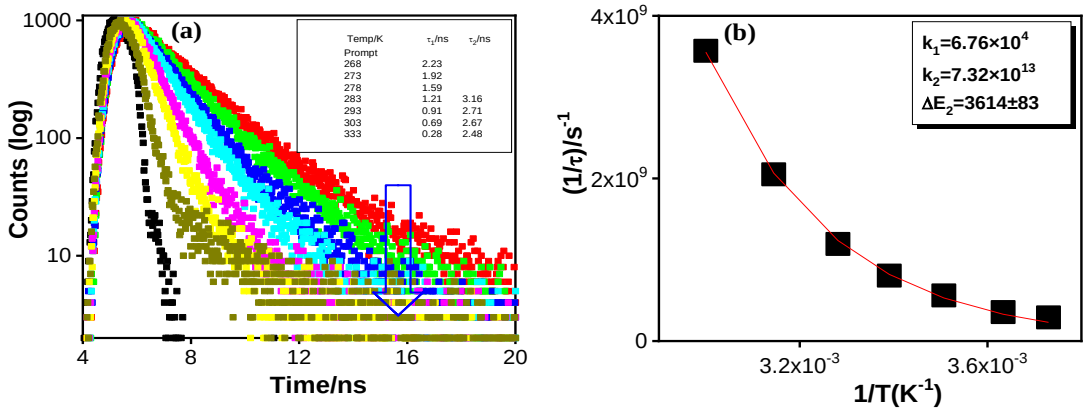

Fig. S9 Change in excited state decay profile of **1H** in MeCN as a function of temperature (a). Non-linear fitting of temperature-dependent lifetime data (b). Inset to figure (b) indicates different parameters.

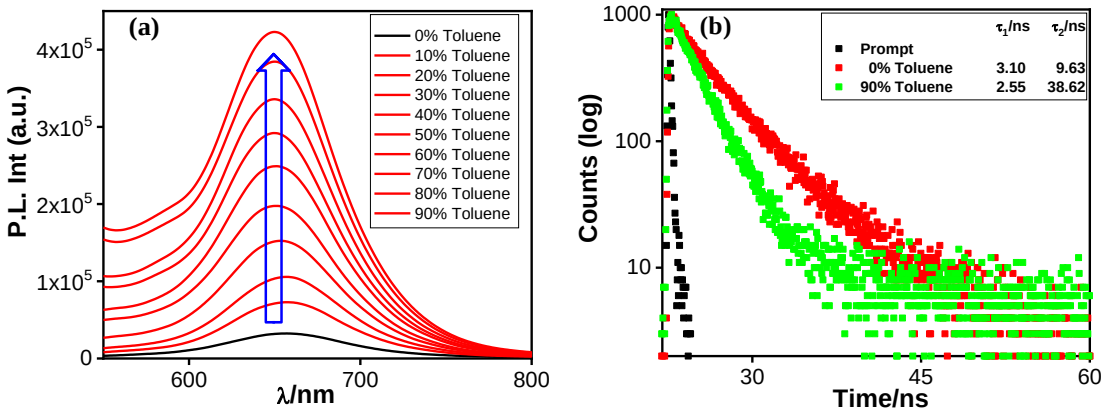

Fig. S10 (a) The emission spectral changes of **1H** upon varying the relative ratio of DMSO and toluene. (b) Decay profile and associated lifetime values for 0% and 90% toluene fraction.

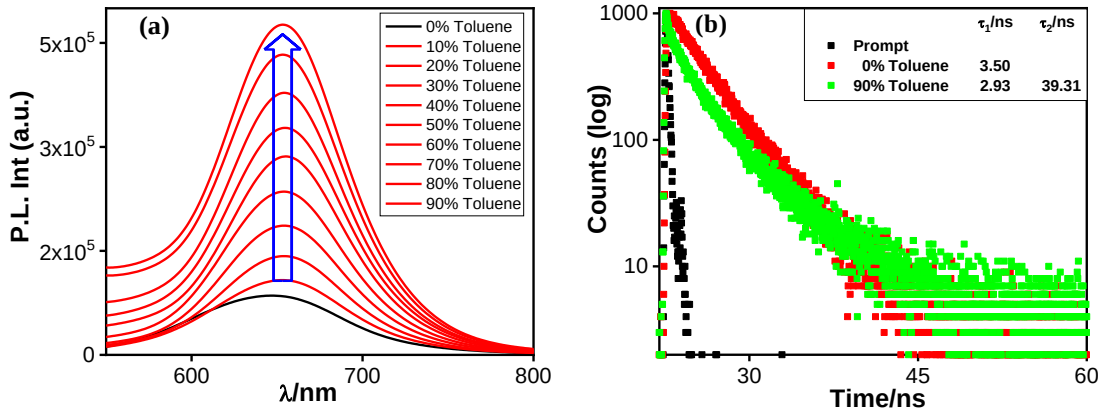

Fig. S11 (a) The emission spectral changes of **2H** upon varying the relative ratio of DMSO and toluene. (b) Decay profile and associated lifetime values for 0% and 90% toluene fraction.

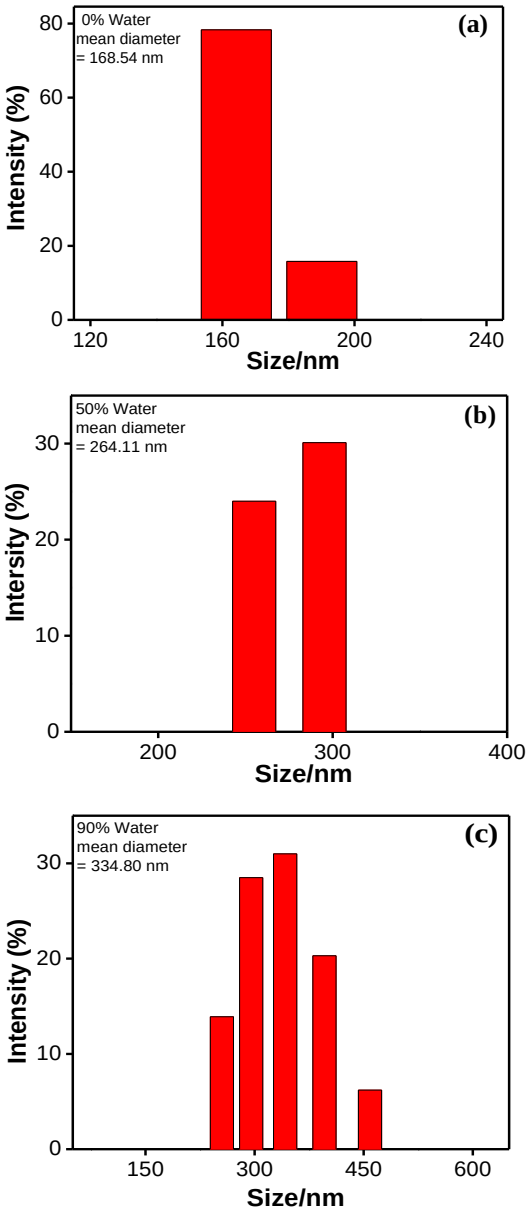

Fig. S12 Change in particle size of **1H** observed through Diffractive Light Scattering (DLS) experiment upon gradual increase of the volume fraction of water {0%-(a), 50%-(b), 90%-(c)} in DMSO.

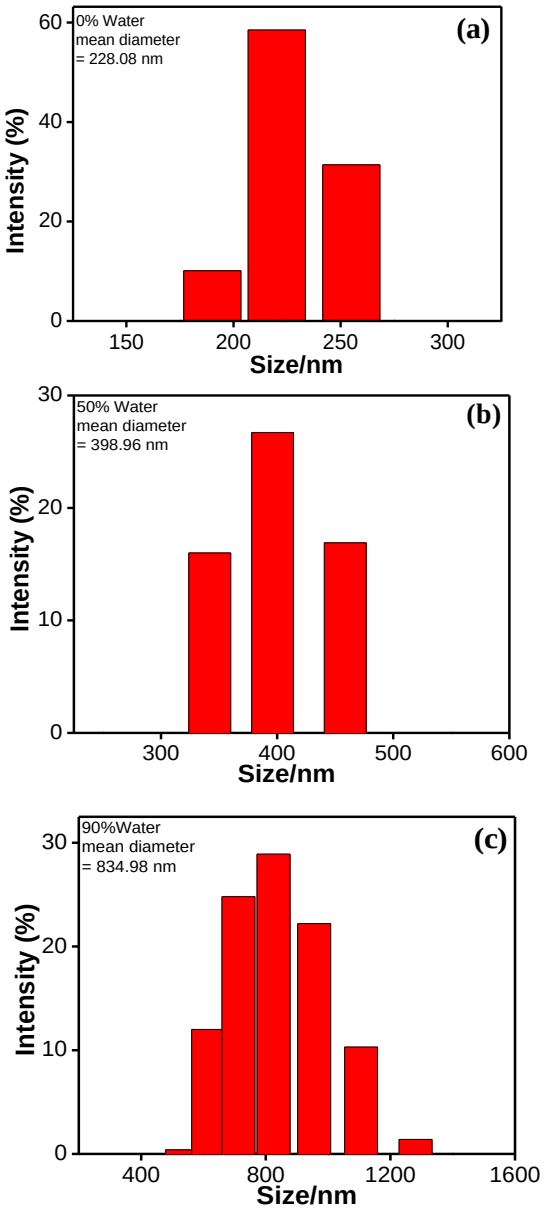

Fig. S13 Change in particle size of **2H** observed through Diffractive Light Scattering (DLS) experiment upon gradual increase of the volume fraction of water {0%-(a), 50%-(b), 90%-(c)} in DMSO.

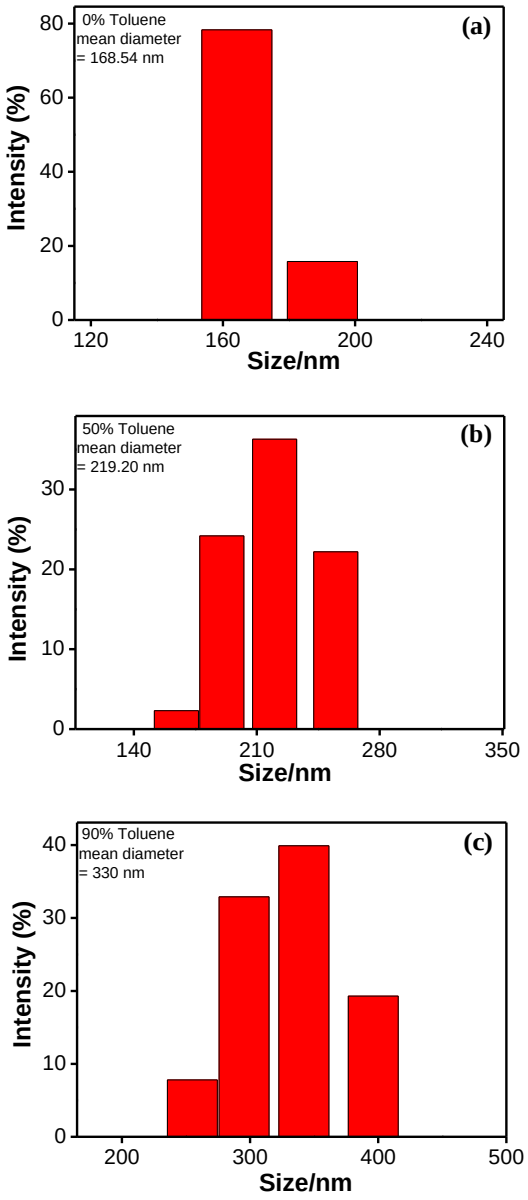

Fig. S14 Change in particle size of **1H** observed through Diffractive Light Scattering (DLS) experiment upon gradual increase of the volume fraction of toluene {0%-(a), 50%-(b), 90%-(c)} in DMSO.

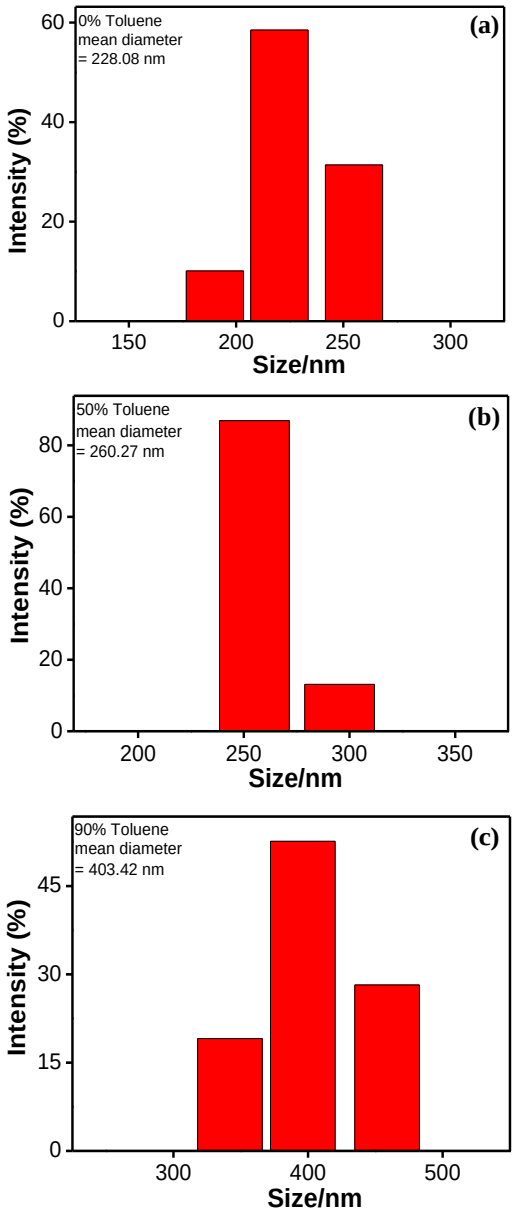

Fig. S15 Change in particle size of **2H** observed through Diffractive Light Scattering (DLS) experiment upon gradual increase of the volume fraction of toluene {0%-(a), 50%-(b), 90%-(c)} in DMSO.

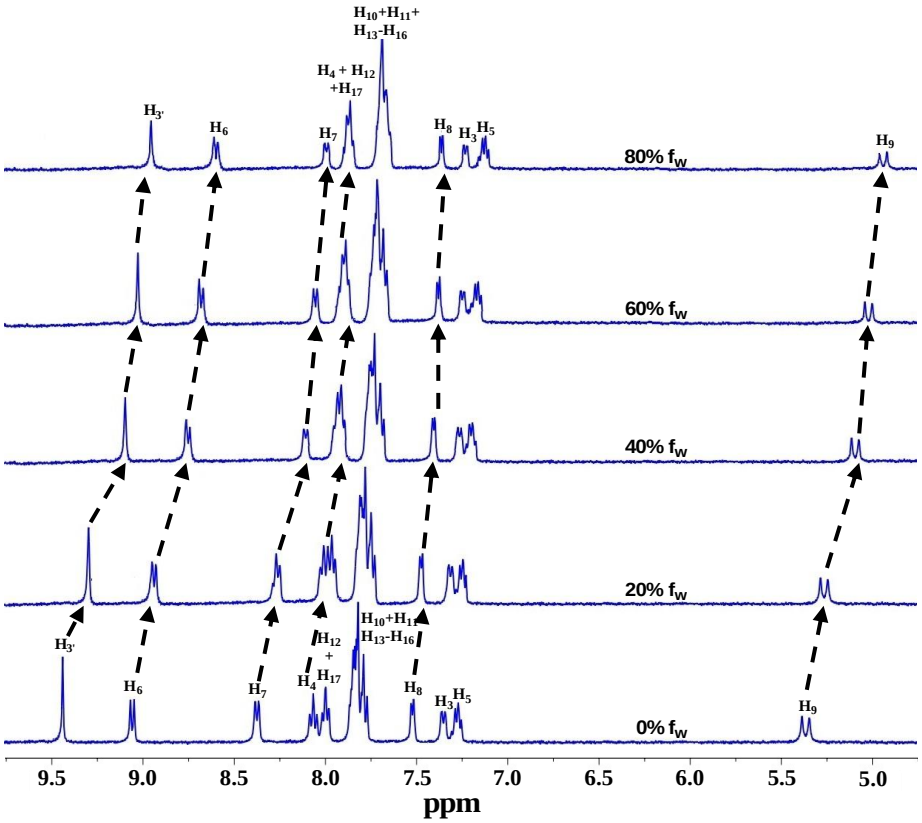

Fig. S16 ^{1}H NMR spectral change of **2H** upon gradual addition of D_2O in DMSO-d_6.

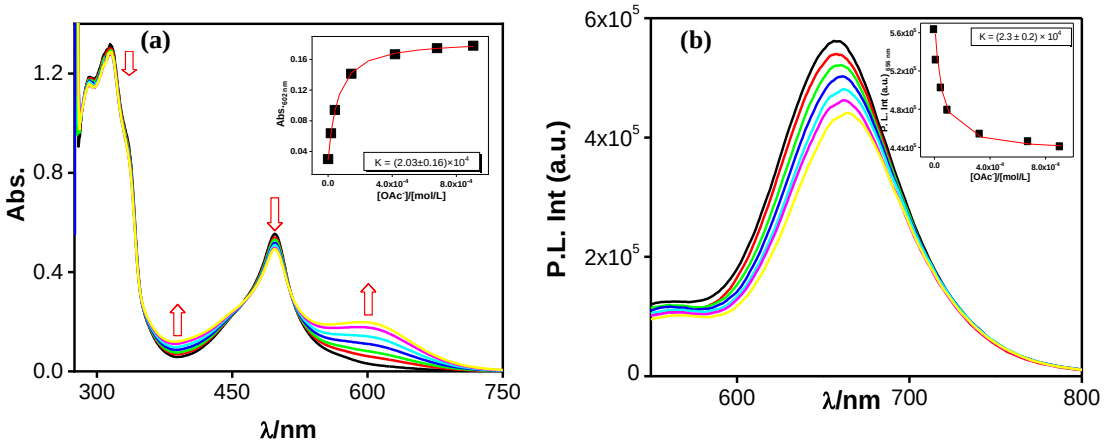

Fig. S17 UV-vis absorption (a) and photoluminescence (λ_{ex}=495 nm) (b) spectral change of **1H** (1.5×10^{-5} M) in dimethylsulfoxide upon gradual addition of OAc^- (up to 5.5 equiv). Insets show the fit of the experimental absorbance and luminescence data to a 1:1 binding profile.

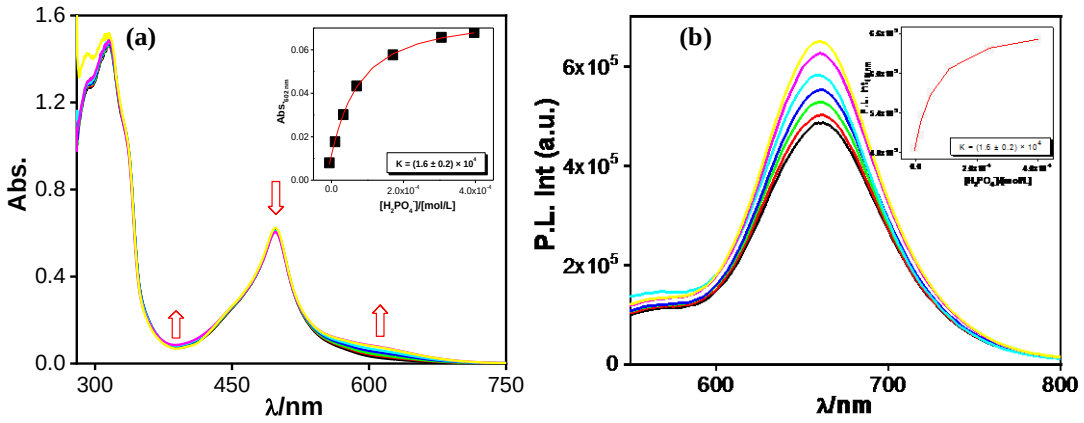

Fig. S18 UV-vis absorption (a) and photoluminescence (λ_{ex}=495 nm) (b) spectral changes of **1H** (1.5×10^{-5} M) in dimethylsulfoxide upon gradual addition of $H_2PO_4^-$ (up to 4.0 equiv). Insets show the fit of the experimental absorbance and luminescence data to a 1:1 binding profile.

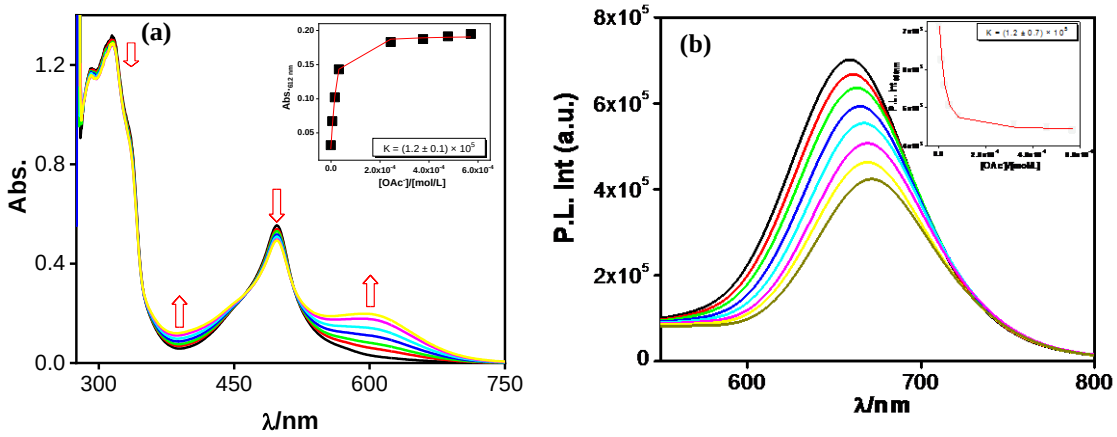

Fig. S19 UV-vis absorption (a) and photoluminescence (λ_{ex}=495 nm) (b) spectral changes of **2H** (1.5×10^{-5} M) in dimethylsulfoxide upon gradual addition of OAc^- (up to 8.5 equiv). Insets show the fit of the experimental absorbance and luminescence data to a 1:1 binding profile.

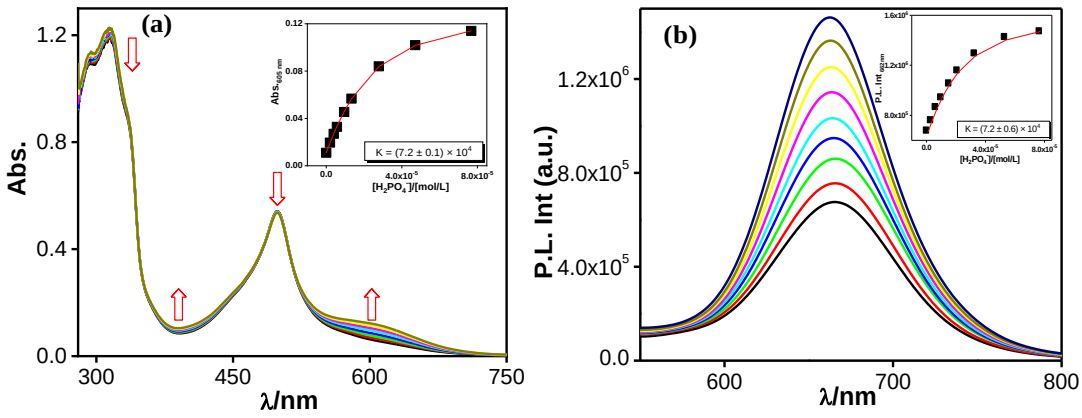

Fig. S20 UV-vis absorption (a) and photoluminescence (λ_{ex}=495 nm) (b) spectral change of **2H** (1.5×10^{-5} M) in dimethylsulfoxide upon gradual addition of $H_2PO_4^-$ (up to 6.0 equiv). Inset shows the fit of the experimental absorbance and luminescence data to a 1:1 binding profile.

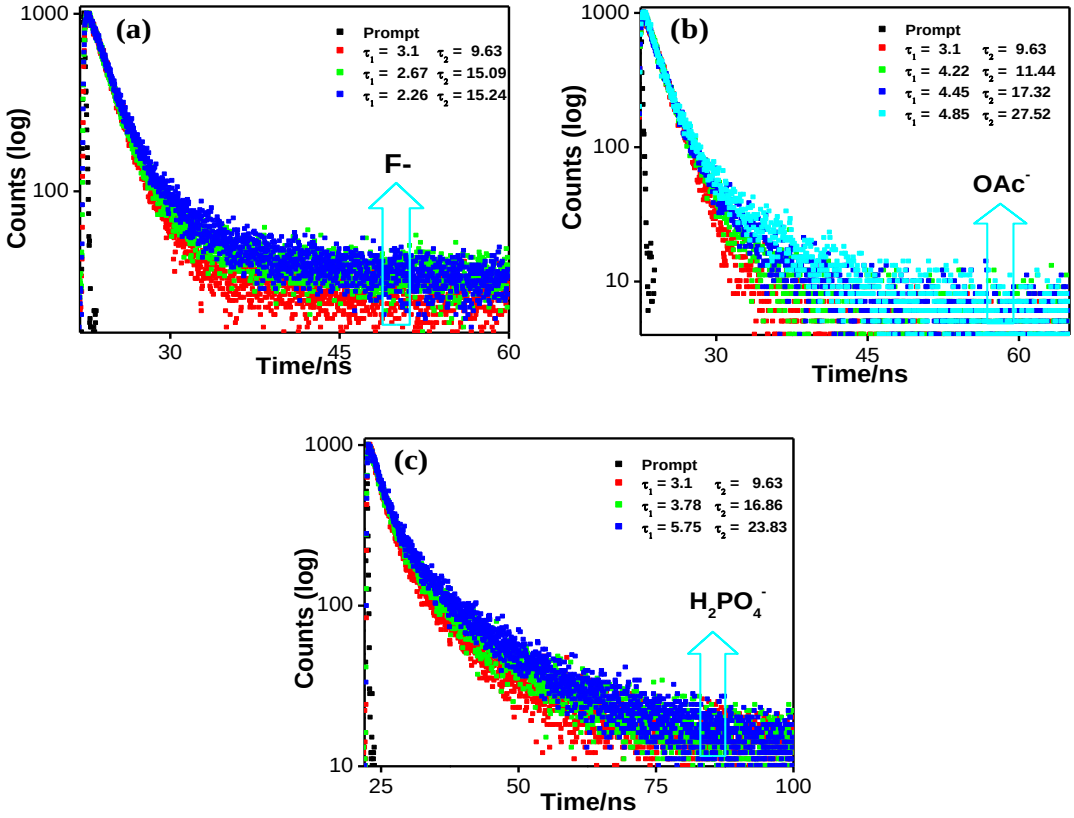

Fig. S21 The change in excited state decay profile of **1H** upon gradual addition of F^- (a), OAc^- (b), $H_2PO_4^-$ (c) in DMSO at RT. The insets show the lifetime values of the complex.

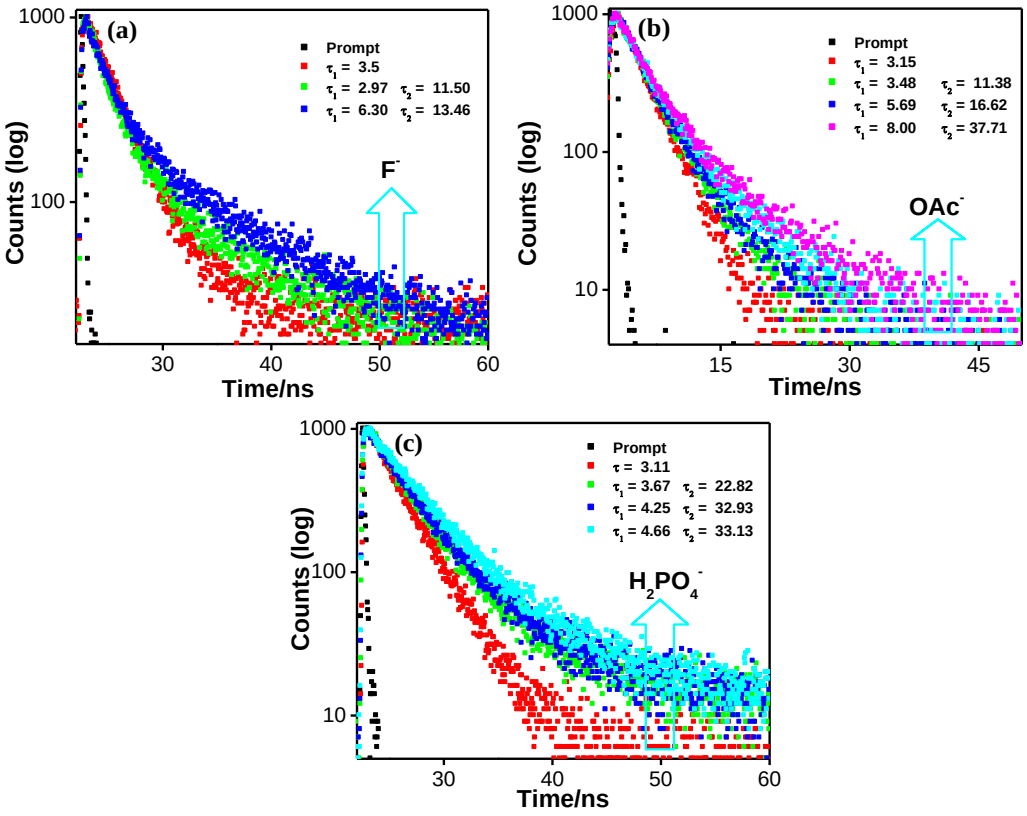

Fig. S22 The change in excited state decay profile of **2H** upon gradual addition of F^- (a), OAc^- (b), $H_2PO_4^-$ (c) in DMSO at RT. The insets show the lifetime values of the complex.

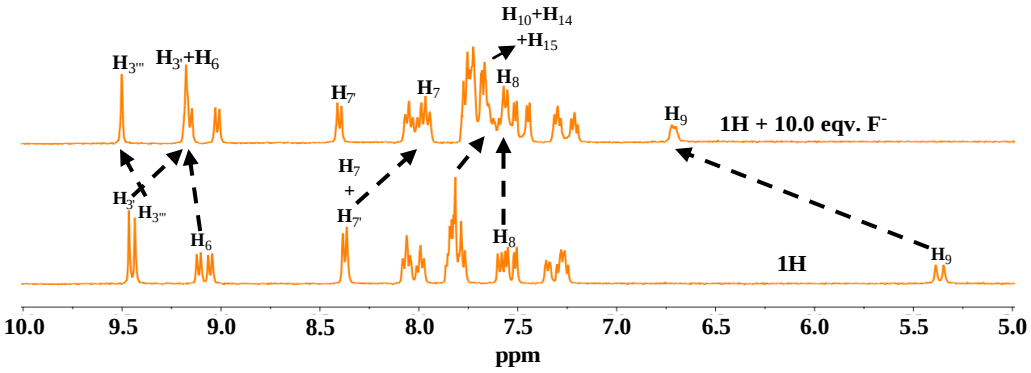

Fig. S23 ^{1}H NMR spectrum of **1H** in absence and in presence of 10.0 equiv. of F^- in DMSO-d_6.

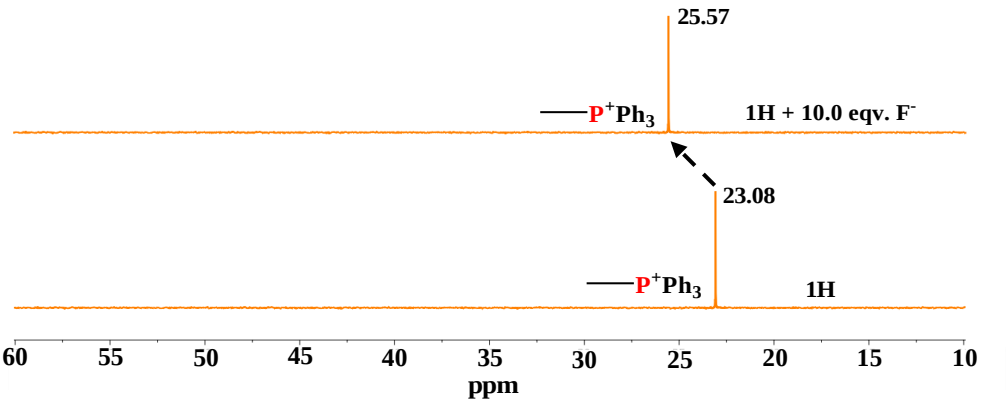

Fig. S24 ^{31}P NMR spectrum of **1H** in absence and in presence of 10.0 equiv of F^- in DMSO-d_6.

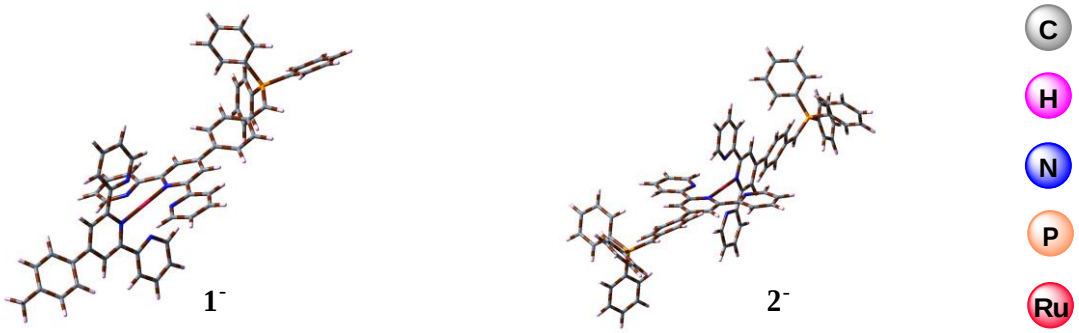

Fig. S25 Optimized structure of the deprotonated forms $\mathbf{1}^-$ and $\mathbf{2}^-$ in DMSO.

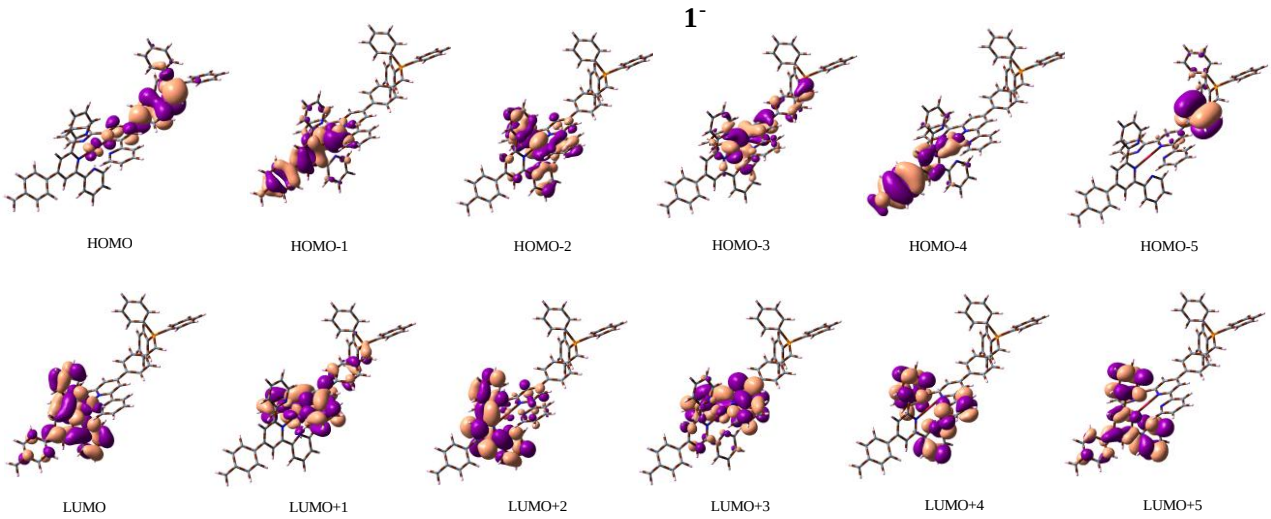

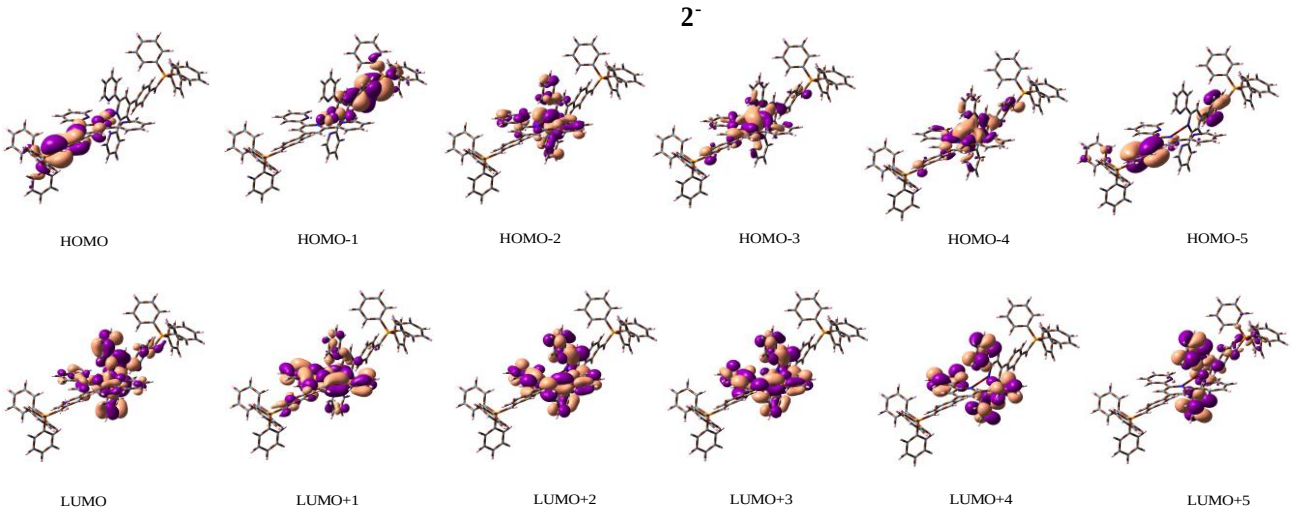

Fig. S26 Schematic drawings of the selective frontier molecular orbitals of deprotonated forms of the complexes (**1**$^{-}$ and **2**$^{-}$**)** in DMSO.

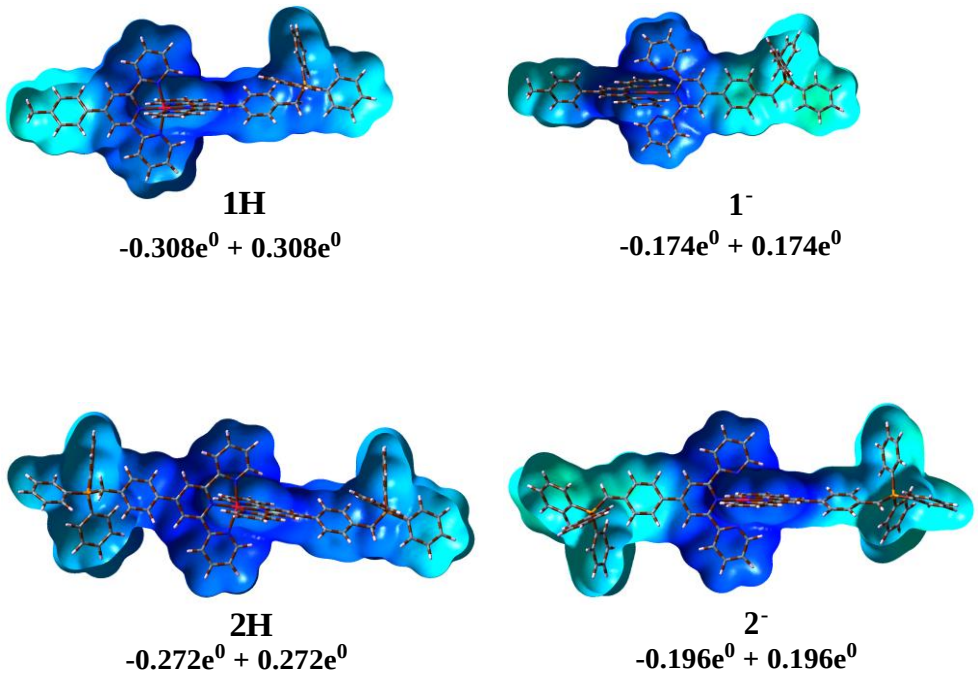

Fig. S27 Electrostatic surface potential plots (ESP) of protonated- (**1H**, **2H**) and deprotonated (**1**$^{-}$, **2**$^{-}$) forms of the complexes in DMSO.

References

S1 C. Bhaumik, S. Das, D. Saha, S. Dutta and S. Baitalik, *Inorg. Chem.* 2010, **49**, 5049-5062.

S2 SAINT (version 6.02), SADABS (version 2.03); Bruker AXS Inc.: Madison, WI, (2002).

S3 M. J. Frisch, G. W. Trucks, H. B. Schlegel, G. E. Scuseria, M. A. Robb, J. R. Cheeseman, G. Scalmani, V. Barone, B. Mennucci, G. A. Petersson, et al. Gaussian 09, revision A.02; Gaussian Inc.: Wallingford, CT, **2009**.

S4 A. D. Becke, *J. Chem. Phys.* 1993, **98**, 5648-5652.

S5 C. T. Lee and W. T. Yang, R. G. Parr, *Phys. Rev. B* 1988, **37**, 785-789.

S6 (a) D. Andrae, U. Haeussermann, M. Dolg, H. Stoll and H. Preuss, *Theor. Chim. Acta.* 1990, **77**, 123-141. (b) P. Fuentealba, H. Preuss, H. Stoll and L. V. Szentpaly, *Chem. Phys. Lett.* 1989, **89**, 418-422.

S7 P. J. Hay and W. R. Wadt, *J. Chem. Phys.* 1985, **82**, 299- 310.

S8 M. E. Casida, C. Jamorski, K. C. Casida and D. R. Salahub, *J. Chem. Phys.* 1998, **108**, 4439-4449.

S9 R. E. Stratmann, G. E. Scuseria and M. J. Frisch, *J. Chem. Phys.* 1998, **109**, 8218-8224.

S10 V. A. Walters, C. M. Hadad, Y. Thiel, S. D. Colson, K. B. Wiberg, P. M. Johnson and J. B. Foresman, *J. Am. Chem. Soc.* 1991, **113**, 4782-4791.

S11 (a) J. Tomasi, B. Mennucci and R. Cammi, *Chem. Rev.* 2005, **105**, 2999-3094. (b) M. Cossi, G. Scalmani, N. Rega and V. Barone, *J. Chem. Phys.* 2002, **117**, 43-54.

S12 M. Caricato, B. Mennucci, J. Tomasi, F. Ingrosso, R. Cammi, S. Corni and G. Scalmani, *J. Chem. Phys.* 2006, **124**, 124520-124530.

S13 B. Mennucci, C. Cappelli, C. A. Guido, R. Cammi and J. Tomasi, *J. Phys. Chem. A* 2009, **113**, 3009.

S14 R. Dennington, T. Keith and J. Millam, Gauss View 3; Semichem, Inc.: Shawnee Mission, KS, 2007.

S15 N. M. O Boyle, A. L. Tenderholt and K. M. Langner, *J. Comput. Chem.* 2008, **29**, 839.